HEMATITE AND GOETHITE INCLUSIONS IN LOW-GRADE DOLOMITIC BANDED IRON FORMATIONS: PHYSICAL PARAMETER EVALUATION TO OPTIMIZE ORE BENEFICIATION

Beate Orberger, Christiane Wagner, Alina Tudryn, Benoît Baptiste, Richard Wirth, Rachael Morgan, Serge Miska

HEMATITE AND GOETHITE INCLUSIONS IN LOW-GRADE DOLOMITIC BANDED IRON FORMATIONS: PHYSICAL PARAMETER EVALUATION TO OPTIMIZE ORE BENEFICIATION

*B. Orberger[1], C. Wagner[2], A. Tudryn[1], B. Baptiste[3], R. Wirth[4], R. Morgan[1] and S. Miska[1]

[1]*Université Paris-Sud, Laboratoire GEOPS, UMR 8148 (CNRS-UPS), Bât. 504, 91405 Orsay, France; (*Corresponding author: beate.orberger@u-psud.fr)*

[2]*Sorbonne Universités, UPMC, Univ Paris 06, CNRS, ISTeP, 4 Place Jussieu, F-75005, Paris, France*

[3]*Sorbonne Universités, UPMC, Univ Paris 06, CNRS, IMPMC, 4 Place Jussieu, F-75005, Paris, France*

[4]*Helmholtz Centre Potsdam, GFZ German Research Centre for Geosciences, Section 3.3, Telegrafenberg, 14473-Potsdam, Germany*

ABSTRACT

Banded iron formations (BIFs) comprise complex textures and mineralogy, which result from fluid-rock interactions related to high and low temperature alteration. The initial iron oxy hydroxide mineralogy and associated phases such as carbonates, quartz, apatite and phyllosilicates were transformed leading to an upgrading of these BIFs into the world's largest source of iron ore. In low-grade BIFs, a large part of the iron is related to micro- and nano- metric iron-bearing inclusions within micrometric quartz and/or carbonates (mainly dolomite). We studied laminated jaspilitic BIF samples from a drill core containing 26.71 wt.% total iron, 0.2 wt.% SiO_2, 0.32 wt.% MnO, 15.46 wt.% MgO, 22.32 wt.% CaO, 0.09 wt.% P_2O_5, < 0.05 wt.% Al_2O_3, 0.15 wt.% H_2O and 34.08 wt.% CO_2 (Àguas Claras Mine, Quadrilátero Ferrífero, Brazil). Bright rose coloured dolomite and quartz bands alternate with massive specular hematite bands. Raman spectroscopy, X-ray diffraction and FIB-TEM analyses reveal that the micro- and nano-metric inclusions in dolomite are mainly hematite and minor goethite, partly occurring as clusters in voids. Curie Balance analyses were carried out at different heating steps and temperatures on whole rock samples and a synthetic mix of decarbonated sample and pure dolomite. X-ray diffraction on the products of the heating experiments shows that that hematite is stable and new phases: magnesioferrite ($MgFe_2O_4$), lime (CaO), periclase (MgO), portlandite ($Ca(OH)_2$) and srebrodoskite ($Ca_2Fe_2O_5$) were formed between 680°C and 920°C. These finding gives hints to optimizing the beneficiation process, as the presence of hydroxyl ions bearing goethite micro- and nanoinclusions lowers the sintering temperature. Prior separation of coarse hematite and barren dolomite and quartz, followed by lower temperature sintering of the inclusion-bearing dolomite/quartz leads to transformations into phases with higher magnetic susceptibilities (such as hematite and magnesioferrite). The entire Fe and Fe/Mg oxide feed (the priorly separated fraction added to the sintered fraction) can then pass through wet-high intensity magnetic separation after crushing.

KEYWORDS

Iron ore, Banded iron formations, Hematite, Goethite, Magnesioferrite, Srebrodoskite, Magnetic separation, Gravitational separation, Iron oxide inclusions, Dolomite.

INTRODUCTION

The iron ore industry faces continuous pressure to reduce the process costs (e.g., grinding below 50 µm to liberate the iron oxides from the gangue in low-grade ores. An ideal blast furnace feed should have about 65% of Fe and an Al_2O_3/SiO_2 ratio of 1, in order to achieve optimized productivity and sufficient slag flow ability, respectively. Lumpy ores (–40 +10 mm) are commercialized. Fines (< 10 mm) are sintered and pelletized (Rao et al., 2009). For example, Vale produces about 40% of pellets out of their total iron ore production of 330 Mt in Brazil (Holmes & Lu, 2015). However, sinter and pellet quality needs to be valued by increasing the Fe content to enhance furnace productivity. Moreover, this valorization will decrease the coke-consumption and thus greenhouse gas emissions (Rao et al., 2009). Iron ores are generally beneficiated by washing, scrubbing, hydrocycloning, gravity and magnetic separation.

From a mineralogical point of view, hematite is preferred over magnetite, as it is easier to reduce than magnetite, although it has a significant lower magnetic susceptibility (magnetite: 625–1,156×10^{-6} m^3/kg, hematite: 0.6–2.16×10^{-6} m^3/kg; Xiong et al., 2015). Hematite is very often associated with hydrohematite and goethite, which have lower magnetic susceptibility than hematite (hydrohematite/goethite: 0.3–1×10^{-6} m^3/kg; hematite: 0.6–2.16×10^{-6} m^3/kg) and lower loose bulk densities (magnetite concentrate; fine ore: 2.5–2.7 t/m^3; hematite: 2–2.6 t t/m^3; martite/goethite: 1.7–1.95 t/m^3; Clout & Manuel, 2015). These heterogeneous physical properties cause difficulties during gravity and magnetic separation.

Low-grade banded iron formations (BIFs) comprise complex textures and mineralogy, which result from fluid-rock interactions varying from low (about 100°C) to high temperature (> 400°C; e.g., Klein, 2005; Morgan et al., 2013; Orberger et al., 2012, 2014). Thus, one sample can host several iron oxide varieties, interstitial to the gangue phases, but also as micro- and nanometric inclusions in gangue minerals. For optimizing the beneficiation, we investigated the numerous iron oxide inclusions, which may represent more than 30% of these ore types by crossing characterization techniques. This complementary mineralogical information can be used for upgrading through beneficiation.

SAMPLE MATERIAL

The studied rock comes from a drill core at 51.6 m depth, sampling the carbonate-rich BIF of the Cauê Formation, Àguas Claras Mine, in the Quadrilátero Ferrífero, Brazil (Rosière et al., 2008 and papers therein). The whole rock sample contains 26.71 wt.% of total iron (expressed as Fe_2O_3), with 0.42 wt.% FeO, 0.2 wt.% SiO_2, 0.32 wt.% MnO, 15.46 wt.% MgO, 22.32 wt.% CaO, 0.09 wt.% P_2O_5, < 0.05 wt.% Al_2O_3, 0.15 wt.% H_2O, and 34.08 wt.% CO_2 (Morgan et al., 2013). On a macro scale, the sample is laminated with alternating pink and dark grey millimetric bands of bright rose coloured dolomite, minor quartz, and massive grey iron oxides (mainly hematite; Figure 1a). Lamination is disrupted by two generations of micrometric veins (parallel and crosscutting to lamination) filled with microcrystalline dolomite (Figure 1a). The dolomite veins are cut by micrometric hematite veins parallel to layering (Figures. 1a and b). The red/pink dolomite bands are predominantly composed of porous dolomite coarse (20 µm) grained dolomite, minor quartz and secondary large (> 100 µm) hematite crystals (Figure 1c). The dolomite includes abundant micro- and nano- metric iron oxy hydroxide inclusions (Figures 1c and d; Morgan et al., 2013).

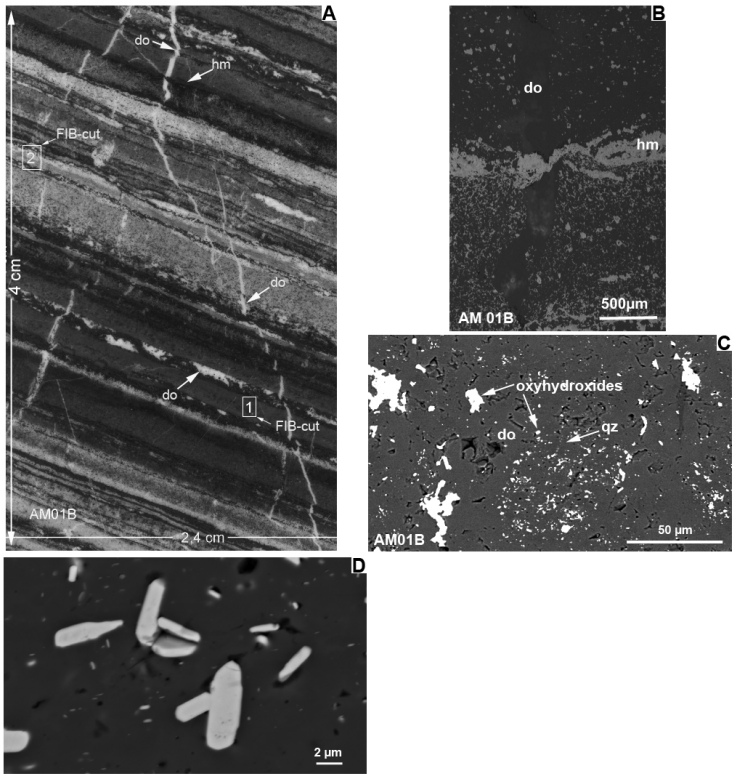

Figure 1 – Main macroscopic and microscopic features of the dolomite BIFs: a) thin section scan showing laminar banding of alternating carbonate (light grey) and hematite (hm, dark grey), and crosscutting and parallel veins of dolomite (do). Squares 1 and 2: location of FIB foils. SEM-BSE images: b) zoom of 2a showing a hematite vein parallel to lamination, which crosscuts a dolomite vein perpendicular to lamination; c) dolomite band: 1) porous dolomite with numerous globular and lath shaped iron oxy hydroxides. 2) coarse dolomite and hematite (10–20 µm); d) zoom of porous dolomite (Figure 1c) showing micro- and nano- metric iron oxy hydroxide inclusions.

Electron microprobe analyses show that the dolomite crystals have a homogeneous composition: on average 29.3 wt.% CaO, 20.9 wt.% MgO, and 0.4 wt.% MnO. The highly variable FeO contents (0.02–7.14 wt.%) are related to the presence of iron oxy hydroxide inclusions within the dolomite crystals. Matrix and vein dolomite have the same chemical composition. Details on the mineral chemistry are described in Morgan et al. (2013).

METHODS

FIB-TEM Analyses

FIB-TEM analyses were performed at the GFZ, Potsdam, Germany, following the technique described in Wirth (2004). Six FIB-foils (15 × 10 µm^2) of 0.15 µm thickness were cut through porous dolomite containing micro- and nano-metric iron bearing inclusions (squares 1, 2; Figure 1a), and coarse grained dolomite containing micrometric iron bearing inclusions. Transmission electron microscopy (TEM) was performed with a Tecnai F20 X-Twin operating at 200 kV with a field emission gun (FEG) as electron source. The TEM is equipped with a Gatan Imaging Filter GIF (Tridiem), a high-angle annular dark field (HAADF) detector and an EDAX analyser. The chemical composition of the iron oxides and the

dolomite was determined in the scanning transmission mode (STEM) by energy-dispersive X-ray (EDX) analyses. The TEM mode was used to assess the bright field (BF) images. Structural data of the investigated phases were derived from selected area electron diffraction (SAED) patterns and from Fast Fourier Transformations (FFT) from high-resolution lattice fringe images.

Curie Balance Analyses

The whole rock sample was crushed to < 100 µm and homogenized. Half of the sample was used chemical and Curie balance analyses, whilst the second half was decarbonated via reaction with pure 100% anhydrous orthophosphoric acid at 80°C for 24 h (McCrea, 1950). After decarbonation, the sample was washed with deionised water until a neutral pH was reached, and dried in an oven at 100°C for 24 h. The thermomagnetic behaviour of the samples was determined on a horizontal force translation Curie balance at the GEOPS laboratory, Université Paris Saclay, France. Analyses were performed in a normal air atmosphere, in a magnetic field of 0.375 T and with a linear temperature increase of 10°C/min.

X-Ray Diffraction Analyses

The X-ray diffraction (XRD) analyses were performed on the same sample material as used for Curie balance experiments. The XRD patterns were recorded with X'Pert Pro PANalytical diffractometer with a Co- and Cu-Kα radiation sources, respectively at the IMPMC laboratory, Université Paris 6, France and the GEOPS laboratory, Université Paris Saclay, France. The analytical conditions were the following: 1) Co-Kα source: 8 h runs, 2 theta range 6°–90°, step size 0.008°, phase identification using ICDD PDF-2 database; 2) Cu-Kα source: 8 or 30 h runs 2 theta range 4°–80°, step size 0.008°, phase identification using COD database.

Micro-Raman Spectroscopy

Raman spectroscopy was performed at the Laboratoire de Sciences de la Terre, ENS-Lyon, Lyon, France, using a Horiba Jobin-Yvon Labram HR800 spectrometer. Oxide phases were characterized through unpolarized Raman spectra excited by the 514.5 nm line of an argon ion laser and collected in a back-scattering geometry with spectral resolution of approximately 4 cm^{-1} (diffraction grating of 600 g/mm). The lateral resolution of the focused laser probe was measured at 1 mm using 100x objective magnitude. The spectral signals were recorded in the range between 150 and 1,800 cm^{-1}. The typical acquisition time was 30–60 s. In order to avoid a laser-induced degradation of the iron phases we used low laser powers (245 µW), as recommended by several authors (de Faria et al., 1997; Gehring et al., 2009; El Mendili et al., 2010), and checked for any sample transformation. Calibration was performed during measurements in a silicon-semiconductor mode at 520.7 cm^{-1}. The Raman spectra were processed by the PeakFit 4.0 (Jandel Scientific) software using Loess smoothing procedure and 2nd-order polynomial function for baseline fitting. The peak-wave numbers were determined assuming a Lorentzian line shape.

RESULTS

FIB- TEM

An HAADF overview of the dolomite FIB-foil 1 (Figure 1a) shows porous dolomite. Two dolomite crystals join at a low angle crystal boundary (Figure 2a). Euhedral crystals (~2 µm) on grain boundaries are hematite, while platelets and lath shaped crystals of clusters are poorly crystalline goethite and/or ferrihydrite based on micro-XRD (Figure 2a). Fe and Mn were detected in dolomite by EDX (Figure 2b), which is in agreement with the electron microprobe analyses showing up to 7 wt.% FeO and 0.4 wt.% MnO on average in dolomite (Morgan et al., 2013). The large (2 µm) euhedral hematite grain shows heterogeneities, whilst the dolomite shows high-dislocation density due to distortions (Figure 2c). BF images of the polycrystalline clusters shown in Figure 2a reveal platy and lath shaped iron oxy hydroxides (30–200 nm in diameter; Figure 2d), which are associated with voids (Figure 2e). These platelets and laths decomposed under the electron beam (inset Figure 2c). FFT diffraction pattern from an HRTEM image of

the laths has the characteristic crystallographic features of both ferrihydrite and goethite: (10-10), (10-12), and (0002) for ferrihydrite, while goethite may be identified by (100), (140) and (040) (Figure 2f). EDX analyses on this iron oxy hydroxide indicate traces of Si (Figure 2g).

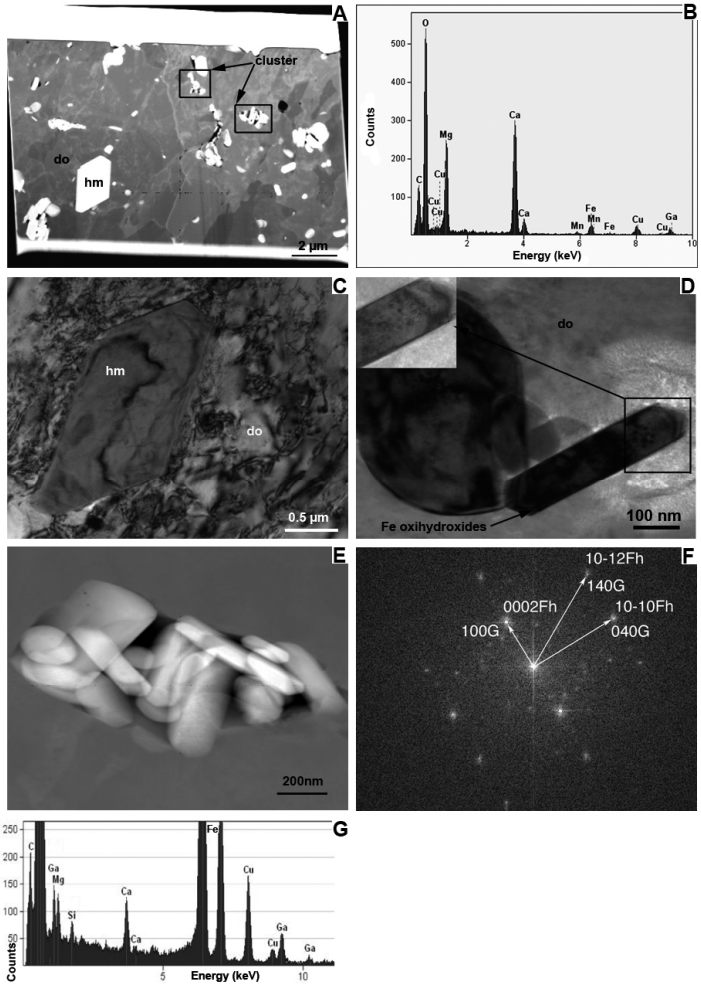

Figure 2 – Micro- and nano- features of a porous dolomite. a) HAADF overview of the dolomite foil showing low angle grain boundary between two dolomite (do) crystals (in middle) with inclusions of euhedral hematite (hm) and clusters of nanometric goethite and ferrihydrite in the porous dolomite; b) EDX analysis on the HAADF image of the dolomite composition; c) BF image of the euhedral hematite showing its heterogeneous contrast and high density of dislocations in dolomite; d) BF image of euhedral iron hydroxide in a cluster. Circular decomposition structures caused by the electron beam are visible in the lath (inset); e) STEM images of the clusters within the porous dolomite (Figure 2a) showing iron hydroxide platelets fully enclosed within dolomite; f) FFT diffraction pattern of the laths shown in Figure 2d indicating both ferrihydrite (Fh) and goethite (G); g) EDX analysis of the laths shows the presence of Si traces.

The FIB-foil 2 was cut in a coarse dolomite from the dark red dolomite band (Figure 3a, square 2). It shows a large euhedral crystal and a small void hosting one euhedral and one subhedral crystal (Figure 3a, square C, and Figure 3c) of hematite according to HREM images and FFT analyses (square 1 and EDX spectrum1 in Figure 3b). The observed angles between (11-25) and (11-21) and between (11-25) and

(0004) are of 33° and 48°, respectively, in agreement with the calculated values (32.09° and 47.5°). This finding confirms the presence of hematite. The dolomite shows a crack in contact to the hematite inclusion (Figure 3b), possibly produced during hematite crystal growth and related thermal differences. The dolomite contains straight dislocation lines (Figure 3b) likely formed below 420°C, the critical temperature where dislocation climbing is observed (e.g., Barber & Wenk, 2001). The two hematite crystals in the void (square C in Figure 3a, and Figure 3c) contain traces of Ca (spectra 1–3 in Figure 3c).

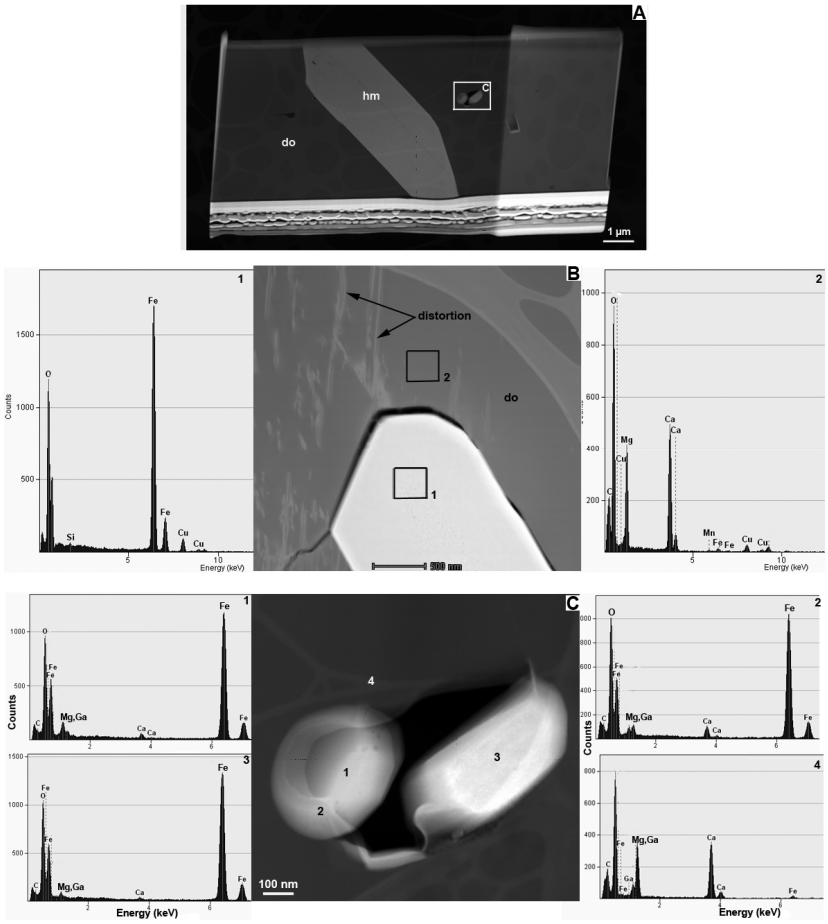

Figure 3 – Micro- and nano- features of coarse dolomite. a) TEM image of a FIB foil cut in the coarse dolomite (square 2 in Figure 1a), showing one euhedral hematite (hm) crystal in dolomite (do) and a void hosting an euhedral and a subhedral crystals. b) detail of the contact between the euhedral hematite crystal (EDX spectrum 1) and the host dolomite (EDX spectrum 2). The dolomite shows straight lines of dislocations and a crystal growth crack. c) zoom of square c in figure 3a showing that the two crystals are hematite (spectra 1 to 3). Note that the dolomite is almost iron free (spectrum 4).

Curie Balance

The whole rock sample heated up to ~750°C, exhibited typical thermomagnetic behaviour for hematite upon heating and cooling, with its Curie temperature at ~680°C. However upon cooling, an additional increase of the magnetisation is observed below ~350°C. This behaviour is not related to the hematite but to a new magnetic mineral, which appears during the experiment (Figure 4a, blue line). As iron oxy hydroxides are included in dolomite, the sample was decarbonated in order to liberate these inclusions. The decarbonated sample was heated up to 900°C and shows the typical thermomagnetic

behaviour of hematite during heating and cooling, (Figure 4a, black line). The new magnetic mineral, which was formed during the whole rock experiment, may thus be related to the dolomitic part of the whole rock sample, or was destroyed during the decarbonation process. This new mineral was formed between 680 and 750°C.

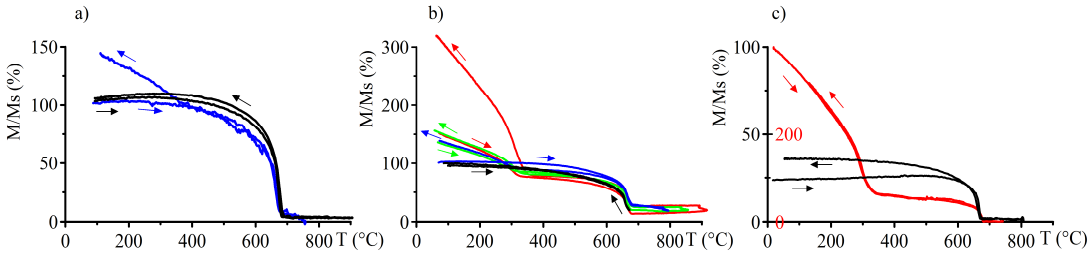

Figure 4 – Curie balance analyses. a) whole rock sample heated up to 750°C (blue line) and decarbonated sample heated up to 900°C (black line), both hold at these temperatures for 30 minutes before cooling; b) whole rock sample heated up to 680°C, cooled and successively heated and being held for 30 minutes at 800, 850 and 920°C before cooling (respectively, black, blue, green and red lines). c) decarbonated sample mixed with standard dolomite and heated up to 800°C (black line) and 920°C, held at 920°C for 30 minutes, cooled and re-heated at 920°C (red line).

In order to determine the temperature interval and conditions in which the new magnetic mineral is formed, Curie balance analyses were performed on (1) whole rock sample and (2) a decarbonated sample mixed with a standard dolomite from GEOPS laboratory. In experiment (1), the whole rock sample was successively heated to ~680°C, cooled and again successively re-heated to ~800, ~850 and ~920°C, and kept constant for ~30 minutes upon reaching the defined temperature before cooling (Figure 4b, black, blue, green and red lines respectively). The whole rock sample heated to 680°C shows the thermomagnetic behaviour for hematite (Figure 4b, black line). However, after heating the whole rock sample to temperatures higher than 680°C, a new magnetic mineral was observed during cooling below ~350°C. This finding indicates that the new magnetic mineral appears at temperature higher than 680°C. Upon each incremental temperature increase, the proportion of the magnetic phase increases (Figure 4b), and is highest for the last step at ~920°C (Figure 4b, red line). In experiment (2) the decarbonated sample was mixed with standard dolomite powder and heated up to ~800 and ~920°C, and maintained at these temperatures for 30 minutes before cooling (Figure 4c). The sample previously heated at 920°C and cooled, was heated again at 920°C (Figure 4c, black line). On heating up to 800°C, only hematite is observed (Figure 4c, red line), but when heated until ~920°C, the sample shows an increase in the magnetisation during cooling below ~350°C.

The new magnetic mineral from both experiments (Figures 4b and c), demagnetises above temperature of ~350°C when heated again, and becomes re-magnetised at the same temperature upon cooling. It can be seen that the new magnetic phase has a far greater magnetisation than the hematite. These experiences show that the formation of the new magnetic mineral results from two processes, which occurred 1) at temperatures higher than 680°C and lower than 900°C, and 2) above 900°C.

X-Ray Diffraction Analysis

XRD experiments have been performed with Co and Cu anodes. In both configurations, XRD measurements on powdered whole rock samples show dolomite and hematite (Figure 5a). XRD analyses (8 h runs) on whole rock samples previously heated and held at ~920°C for 30 minutes show hematite as in Figure 5a, lime (CaO), periclase (MgO) and portlandite ($Ca(OH)_2$; (Figures 5b and c,. Magnesioferrite ($MgFe_2O_4$) was identified with low intensities at the diffraction peaks at 2.52 Å [I = 100 (311)], 1.48 Å [I = 46 (440)], 2.96 Å [I = 36 (220)]. However, the XRD analyzes with Cu anode on a whole rock sample (run for 30 h, held at ~920°C for ~3 h) show higher intensities for the major peaks of magnesioferrite (Figure

5d). Furthermore, srebrodolskite ($Ca_2Fe_2O_5$) was identified by the peaks at 2.67 Å [I = 100 (141)], 2.71 Å [I = 43.62 (200)] and 1.95 Å [I = 39.08 (202)].

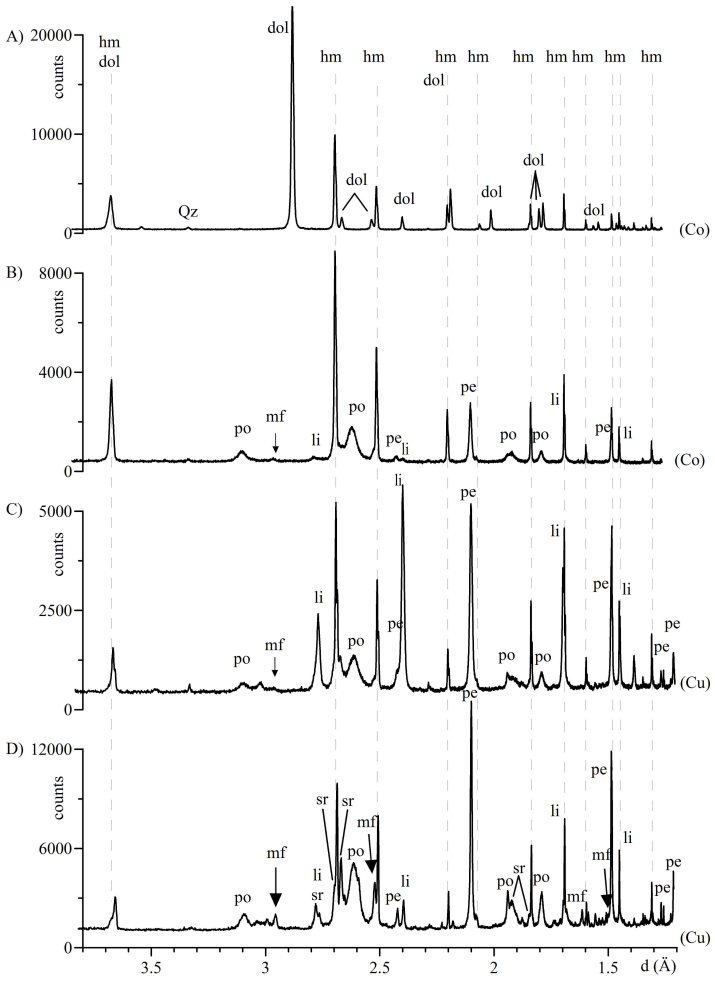

Figure 5 – XRD spectra: a) whole rock sample, measured with Co anode; b), c), d): residue produced from the Curie balance analysis held at ~920°C for b) 30 minutes, Co anode; c) 30 minutes, Cu anode; d) 3 h, Cu anode. Co – cobalt, Cu – copper, hm – hematite, dol – dolomite, li – lime, pe – periclase, po – portlandite, mf – magnesioferrite, sr – srebrodolskite. The x axis are presented in distance (Å).

Micro-Raman Spectroscopy

Raman spectra were collected from the dolomitic band on iron minerals within coarse dolomite, and on micrometric iron oxy hydroxide inclusions from porous dolomite and quartz. In all cases, the spectra show bands at 224–226, ~ 300 cm^{-1}, 411–414, 498–502, 611–621, 668–673 and 1,321–1329 cm^{-1} (Figure 6). The band at ~ 300 cm^{-1} is deconvoluted in two bands at 290–293 and 299–306 cm^{-1}, the latter one usually appears on the flank of the stronger ~ 290 cm^{-1} band. In some spectra an additional band at 244–247 cm^{-1} appears. This combination of bands is typical of hematite (e.g., de Faria et al., 1997; Hanesh, 2009). The spectra from the different host minerals do not show any difference, only hematite was recorded.

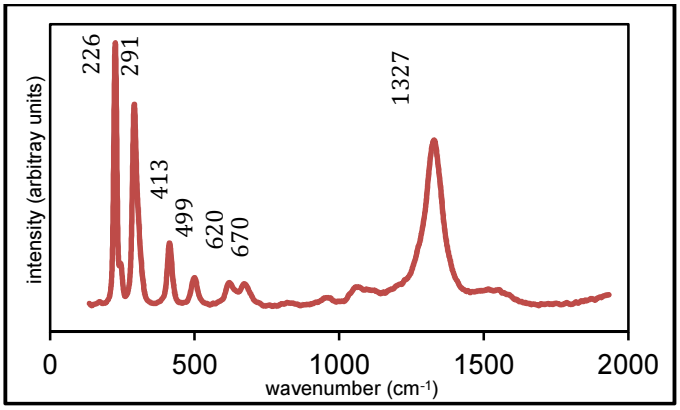

Figure 6 – Raman spectrum of hematite from an inclusion in the porous dolomite

DISCUSSION AND CONCLUSIONS

This study shows that the detailed characterization through cross-method analysis and understanding of the physical and chemical properties of the feed are necessary to design a successful process flow sheet, which provides optimized products for the blast furnaces.

In order to design an optimal process flow sheet, the following parameters have to be taken into consideration. Three dolomite types are present: 1) Porous dolomite about 10 µm large grains rich in iron oxy hydroxide inclusions (Figure 1c); 2) Coarse grains (30–50 µm) free of iron hydroxide but rich in hematite inclusions; 3) Parallel and cross banding coarse grained dolomite in veins or lenses free of iron oxy hydroxide inclusions. The iron oxides are hematite, no maghemite or martite was observed, unlike for example in BIFs from the Indian Dharwar Craton and from Brazilian soils, respectively (Orberger et al., 2014). Four types of hematite are distinguished: 1) euhedral lath shaped inclusions in porous or coarse dolomite several tens to hundreds of nm long; 2) needle shaped (specularites), 30–50 µm long, 2–5 µm wide, oriented along grains boundaries; 3) several tens of µm large agglomerates of heterogeneous shapes. Types 2 and 3 are interstitial to coarse dolomite grains; and 4) massive veins.

For the first time, the presence of iron oxy hydroxides as euhedral clusters in voids from the porous dolomite was evidenced by our cross-method approach. Only FIB-TEM analyses coupled with EDX and micro-XRD analyses allow their mineralogical characterization. It should be noticed that the clusters are still present because the goethite and/or the ferrihydrite contain traces of silica known to increase their stability (Cornell & Schwertmann, 2003). Indirect hints to the presence of iron hydroxides within the dolomite were provided by the heating experiments on the whole rock sample at temperatures between ~680°C and ~900°C, which produced magnesioferrite (+ lime, periclase and srebodolskite). Our experiments show that the magnesioferrite formation at such temperatures is only possible in dolomite if a hydrated phase, such as goethite is present. Iron oxy hydroxides (hematite in globular textures and lath shaped goethite) were also observed in cavities of micro quartz in BIFs from the Indian Dharwar Craton (Orberger et al., 2012). Furthermore, for the first time growth cracks around micrometric hematite inclusions were observed in coarse dolomite.

In order to valorize these iron of these micro-and nanoinclusions in dolomite and/or quartz, this fraction could be first separated from the coarse hematite (specularite and hematite agglomerates, types 2 and 3) and the barren gangue by two successive gravity separation processes (spiraling and jigging) after crushing at about 50 µm. During this crushing process, the thermal cracks observed around hematite inclusions in coarse dolomite may propagate and liberate at least part of the inclusions. The fertile dolomite/quartz with goethite and hematite inclusions should be hydrocycloned in case of abundant slime material (e.g., clay minerals). For information, the here studied sample contains chlorite (Morgan et al.,

2013), while in siliceous BIFs, kaolinite and illite are present (Orberger et al., 2012). To liberate the micro- and nanometric inclusions, a sintering step will transform the goethite into hematite and/or magnesioferrite. The presence of hydroxyl ions goethite inclusions lowers the sintering temperature and, thus, saves energy and reduces operational costs (OPEX). Coarse priory separated hematite can then be added to the sintered hematite/magnesioferrite, and this feed can then pass through wet-high intensity magnetic separation (e.g., Das et al., 2007; Mishra et al., 2007).

ACKNOWLEDGMENTS

The authors gratefully acknowledge the mining companies Vale and Llhoist do Brazil for providing their permission to study the samples as well as logistical and practical support and information. We thank the Laboratoire de Géologie de Lyon (ENS-Lyon) to give us access to the national Raman instrument supported by the Institut national des Sciences de l'Univers (INSU), CNRS. Carlos Rosière (UFMG, Belo Horizonte, Brazil) is thanked for logistical help during field work, Anja Schreiber (GFZ, Germany) for the FIB-TEM preparation, Gilles Montagnac (ENS-Lyon) for technical help with the Raman analyses and Luce Delabesse (GEOPS-UPS, France) for image preparation We thank Rachel Morgan from Canberra, Australia for the English revision of the paper. This study was funded by PNP, COFECUB-CAPES, the Brazilian VALE/CNPq project 5503482010-7.

REFERENCES

Barber D.J., & Wenk H-R. (2001). Slip and dislocation behaviour in dolomite**.** *Eur J Mineral 13*, 221–243.

Clout, J. M. F., & Manuel, J. R. (2015). Mineralogical, chemical and physical characteristics of iron ore. In L. Limung (Ed.). *Iron ore: Mineralogy, Processing and environmental sustainability*. pp. 45–84. Amsterdam: Elsevier.

Cornell R., & Schwertmann U. (2003). *The iron oxides: structure, properties, reactions, occurrences and use*. New York Wiley-VHC.

Das, B., Prakash, S., Das, S. K., & Reddy, P. S. R (2007). Effective beneficiation of low grade iron ore through jigging operation. *Journal of Minerals & Materials Characterization & Engineering,7*, *1*, 27–37.

De Faria, D. L. A., Venancio-Silva, S., & de Oliveira, M. T. (1997). Raman microspectroscopy of some iron oxides and oxyhydroxides. *Journal of Raman Spectroscopy, 28*, 873–878.

El Mendili, Y., Bardeau, J. F., Randrianantoandro, N., Gourbil, A., Greneche, J. M., Mercier, A. M., & Grasset, F. (2010). New evidence of *in situ* laser irradiation effects on γ-Fe_2O_3 nanoparticles: a Raman spectroscopic study. *Journal of Raman Spectroscopy, 42*, 239–242.

Gehring, A. U., Fischer, H., Louvel, M., Kunze, K., & Weidler, P. G. (2009). High temperature stability of natural maghemite: a magnetite and spectroscopic study. *Geophysical Journal International, 179*, 1361–1371.

Hanesh, M. (2009). Raman spectroscopy of iron oxides and (oxy) hydroxides at low laser power and possible implications in environmental magnetic studies. *Geophysical Journal International, 177*, 941–948.

Holmes, R.J., & Lu, L. (2015). Introduction: overview of the iron ore industry. In L. Limung (Ed.). *Iron ore: Mineralogy, Processing and environmental sustainability*. pp. 1–42. Amsterdam: Elsevier.

Klein, C. (2005). Some Precambrian banded iron-formations (BIFs) from around the world: Their age, geologic setting, mineralogy, metamorphism, geochemistry, and origins, *American Mineralogist*, *90*, 1473–1499.

McCrea, J.M. (1950). On the isotope chemistry of carbonates and a paleo-temperature scale. *J Chem Phys., 18,* 849–857.

Mishra, B. K., Reddy, P. S. R., Das, B., Biswal, S. K., Prakash, S., & Das, S. K. (2007). Issues relating to characterization and beneficiation of low grade iron ore fines. *Steelworld, 11*, 34–36.

Morgan, R. R., Orberger, B., Rosière, C. A., Wirth, R., da Mota Carvalho, C., & Bellver-Baca, M. T. (2013). The origin of coexisting carbonates in banded iron formations: A micro-mineralogical study of the 2.4 Ga Itabira Group, Brazil. *Precambrian Research*, *224*, 491–511.

Orberger, B., Wagner, C., Wirth, R., Quirico, E, Gallien, J. P., Derré, C., … Rouchon, V. (2012). Origin of iron-oxide spherules in the banded iron formation of the Bababudan Group, Dharwar Craton, Southern India. *Journal of Asian Earth Sciences, 52*, 31–42.

Orberger, B., Wagner, C., Tudryn, A., Wirth, R., Morgan, R., Fabris, J. D., & Rosière, C. (2014). Micro- to nano- scale characterization of martite from a banded iron formation in India and a lateritic soil in Brazil. *Physics and Chemistry of Minerals. 41, 9*, 651–667.

Rao, D. S., Kumar, T. V., Subba Rao, S., Prabhaka, S., & Bhaskar Raju, G. (2009). Mineralogy and Geochemistry of a Low Grade Iron Ore Sample from Bellary-Hospet Sector, India and their Implications on Beneficiation. *Journal of Minerals & Materials Characterization & Engineering, 8*(2), 115–132.

Rosière, C. A., Spier, C. A., Rios, F.J., & Suckau, V E. (2008). The Itabirites of the Quadrilátero Ferrífero and related high-grade iron ore deposits: an overview. *SEG Reviews, 15*, 223–254.

Xiong, D., Lu, L., & Holmes, R.J. (2015). Developments in the physical separation of iron ore: magnetic separation. In L. Limung (Ed.). *Iron ore: Mineralogy, Processing and environmental sustainability*. pp. 283–307. Amsterdam: Elsevier.